Scanning Microscopy

Volume 4 | Number 3 Article 10

7-21-1990

Scanning Ion Microprobe Assessment of Biological Sample Preparation Techniques

Phillippe Hallegot
The University of Chicago

Chantal Girod
The University of Chicago

Riccardo Levi-Setti
The University of Chicago

Scanning Microscopy, Vol. 4, No. 3, 1990 (Pages 605-612) 0891-7035/90$3.00+.00
Scanning Microscopy International, Chicago (AMF O'Hare), IL 60666 USA

SCANNING ION MICROPROBE ASSESSMENT OF BIOLOGICAL SAMPLE PREPARATION TECHNIQUES

Philippe HALLEGOT*, Chantal GIROD and Riccardo LEVI-SETTI

The Enrico Fermi Institute, The University of Chicago, 5640 S. Ellis Avenue, Chicago, Illinois 60637, USA.

(Received for publication March 18, 1990, and in revised form July 21, 1990)

Abstract

Different preparation techniques for high lateral resolution scanning ion microprobe imaging of biological samples have been investigated. The sharpest histological maps are obtained from chemically fixed and plastic embedded specimens. It is often problematic to correlate ultrastructure and bioaccumulation from analysis of frozen cut and lyophilized sections. The best compromise is to resin-embed frozen samples in order to get a perfectly flat section from tissue where the *in vivo* ion distribution is maintained. Use of the University of Chicago Ion Microprobe gave us the ability to observe the relative ion translocations induced during sample preparation. As an example, we show the rapid decrease of intracellular K^+/Na^+ ratio through a fast frozen blood droplet.

Key words: Secondary Ion Mass Spectrometry, Scanning Ion Microprobe, High Lateral Resolution Isotope Imaging, Sample Preparation, Diffusible Ions, Cryofixation, Lyophilisation, Sample Embedding, Microquantitation, Elemental Translocation.

*Address for correspondence:
Philippe HALLEGOT
The Enrico Fermi Institute
The University of Chicago
5640 S.Ellis Avenue
Chicago, Illinois 60637,USA.

Phone No: (312)-702-7586.

Introduction

Using a high lateral resolution scanning ion microprobe at the University of Chicago (University of Chicago Scanning Ion Microprobe: UC-SIM) (Levi-Setti et al., 1985; Levi-Setti et al., 1988a), we analyzed biological samples prepared following various protocols in order to test their ability to reveal biological structures and preserve the ion content of these structures. A way to evaluate the preservation of the *in vivo* ion content is to acquire and compare Na^+ and K^+ secondary ion signals from cells (Chandra and Morrison, 1985). We froze a human blood droplet and measured the K^+/Na^+ ratio from the surface to the interior of the sample every 2 µm over a depth of 55 µm. Two measurement techniques were used: (i) local counting from corresponding areas in simultaneously acquired K^+ and Na^+ maps (Chabala et al., 1989), (ii) acquisition of mass spectra during the scanning of preselected areas of the sample.

To prepare the sample for sectioning, we embedded the frozen blood droplet with plastic following a protocol similar to that previously used for conventional Secondary Ion Mass Spectrometry (SIMS) by Burns and File (1986). With the UC-SIM we can investigate plastic impregnation and ion translocations during the embedding procedure. Our study also points out what surface modifications occur during the scanning of a biological sample by the ion probe, preliminary to analysis by SIMS.

Materials and Methods

Sample preparation.

Chemical fixation. Tissues were fixed with 1.5% glutaraldehyde in 0.1 M cacodylate buffer (pH 7.4), washed in the cacodylate buffer, and air dried (in situ fixed cell cultures) or dehydrated in ethanol (tissues to be embedded in Epon or Spurr). 1 µm thick sections from embedded samples were deposited on gold slides (purity 99.999%).

Cryofixation. The preparations were dipped into a nitrogen slush bath at a speed of 2 m/s to a depth of 5 cm. Frozen samples were then transferred under liquid nitrogen into a lyophilizer, maintained 24 hours at a temperature of -55°C and a pressure of 0.5 millitorr , and, still under vacuum, allowed to reach room temperature in 12 hours. After lyophilization, these were embedded with standard hardness Spurr resin (Spurr, 1969) under a 300 torr vacuum during 24 hours at 20°C, then cured 18 hours at 70°C. The low viscosity of Spurr resin makes it suitable for tissue embedding without requiring the use of an intermediate solvent. 1 µm thick sections were dry cut with a glass knife using a Sorvall microtome. Sections were collected with an ultrathin needle

and deposited onto 50 μm thick gold slide (purity 99.999%) on which they were dry pressed to make them adhere to the slide.

Prior to analysis, all specimens were covered by a 5 nm thick gold layer deposited by plasma sputtering. During analysis, after the very first probe scans, a window is sputtered-open in this gold layer, presenting the biological sample surface to the ion beam. The conductive gold layer, which is still surrounding the scanned area, prevents charging effects.

Scanning Ion Microprobe.

The principles of Secondary Ion Mass Spectrometry (SIMS) (Castaing et al., 1960; Castaing and Slodzian, 1962) and its application to biology (Burns, 1982; Burns, 1988; Galle,1982; Galle et al., 1983; Levi-Setti, 1988b) have been extensively described. To summarize: a primary ion beam is used to bombard a sample which is consequently sputter-eroded. The constituent elements of the eroded volume of the sample, ejected as ions, are collected to form the secondary ion beam. This is subsequently analyzed by mass spectrometry to separate ions according to their m/Z ratio. It is then possible (by selecting a given m/Z ratio) to get, through the imaging mode of the instrument, any ion distribution on the sample surface. The UC-SIM uses a Ga^+ primary beam extracted from a liquid metal ion source. This high brightness source yields a finely focused ion probe still carrying primary current large enough to perform efficient SIMS analysis for most elements of biological interest; using the UC-SIM, a 20 nm diameter probe has been achieved (Levi-Setti et al., 1988a). In this study, a probe diameter of 50 to 90 nm carrying a 30 to 70 pA current has been used. During the scanning of the sample by the probe, secondary ions emitted from the eroded surface are collected and subsequently mass filtered through an RF quadrupole. The mass-resolved signal is used to construct analytical maps which are stored in the digital memory of a KONTRON image processing system or to get a mass spectrum for a chosen mass range.

Results

Study of biological sample structures.

Initial process: ion-induced erosion. Fig.1a shows the topography of a fibroblast nucleus with its two nucleoli in a mass-unresolved, secondary ion image. The sample was fixed with glutaraldehyde and air dried. After 26 minutes of erosion using a 30 pA probe current, the scanned area of 20 μm x 20 μm (Fig.1b) presented few modifications. However, a microrelief appeared due to differential sputtering of the cellular material. The shallow depression due to erosion is well highlighted by the larger field of view of Fig.1c. We estimate that about 10 to 15 nm of the biological sample were eroded in 500 s when a 30 pA Ga^+ probe scanned over a 20 x 20 μm area was used.

Because of this low erosion rate, serial maps, acquired from a particular target region of the section and corresponding to different isotopes, could easily be correlated.

Artifacts due to rough sample surface. In Fig.2a (topographic map, 20 μm x 20 μm) a 2 μm thick section was cut from a plastic embedded pellet of murine erythroleukemic cells. A regular compression of the sample during the sectioning produced a section of periodically uneven thickness. The relief, that appeared on the cellular material, generated a line pattern due to edge effects on the analytical

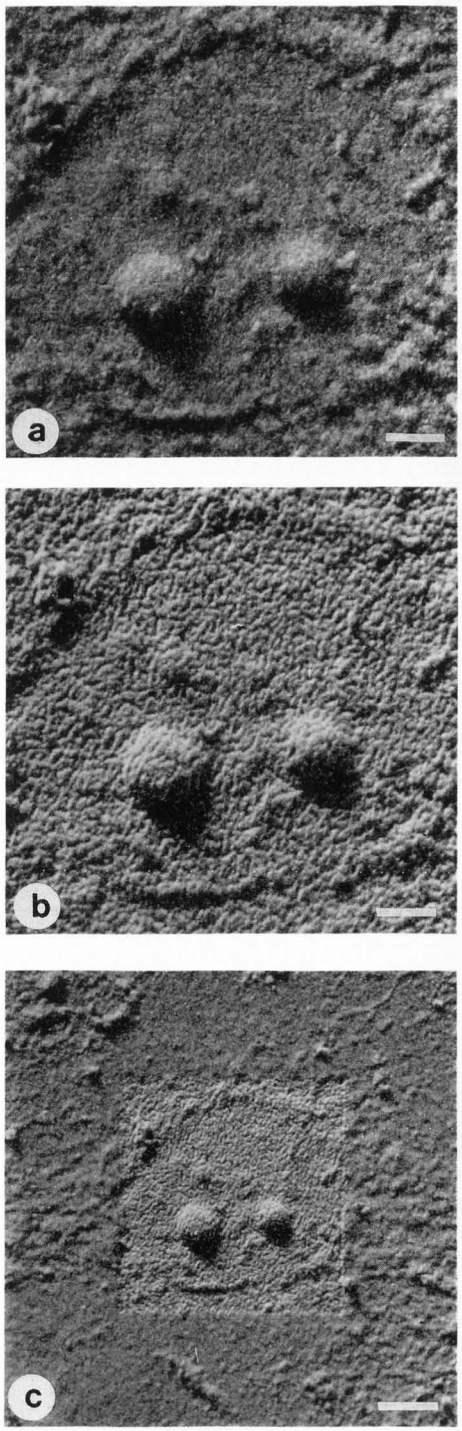

Figure 1. Erosion of a fibroblast nucleus under a 40 KeV gallium probe scan.
Topographic images using secondary electrons.
1024 x 1024 pixels, probe current 30 pA.
a: topography of the nucleus before erosion; nucleoli and nucleus boundaries are clearly visible. Bar = 2.5 μm.
b: image of the same nucleus after 26 minutes of erosion; a microrelief has been generated by the probe. Bar = 2.5 μm.
c: large field of view showing the low eroded volume of nucleus at the end of the scanning. Bar = 5 μm.

map of CN^- (Fig.2b). As a reference, Fig 2c is a CN^- map from a perfectly flat 1 μm-thick section which did not exhibit any edge effect.

Good structure recognition from chemically fixed and plastic embedded sample. Analytical maps at mass 26 (CN^-, mainly originating from proteins (Quettier and Quintana, 1979)) can be used to image the tissue histology. A sample of hairless rat skin was glutaraldehyde fixed, embedded in Epon, and cut (Fig.3); the CN^- map acquired from this section revealed extremely sharp histological details, even at the ultrastructural level, in the stratum corneum, epidermis and dermis. The high counting statistics at mass 26, from embedded samples, always permit the acquisition of images (512 x 512 pixels) with a spatial resolution that reaches the probe diameter size, for an acquisition time which does not exceed 525s and a scanned area of 20 to 40 μm^2 (Chabala et al., 1988).

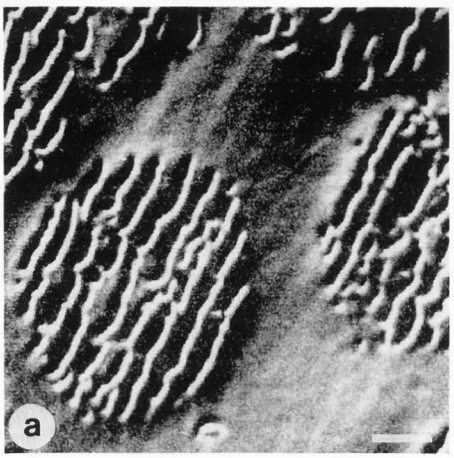

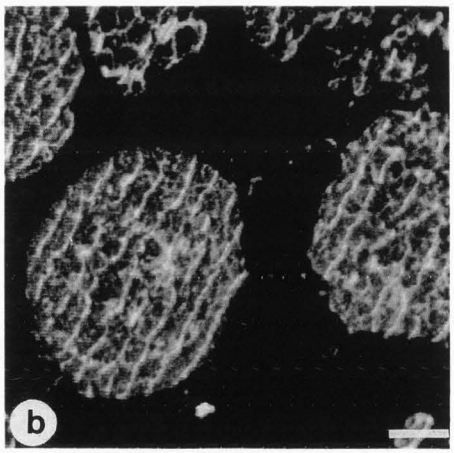

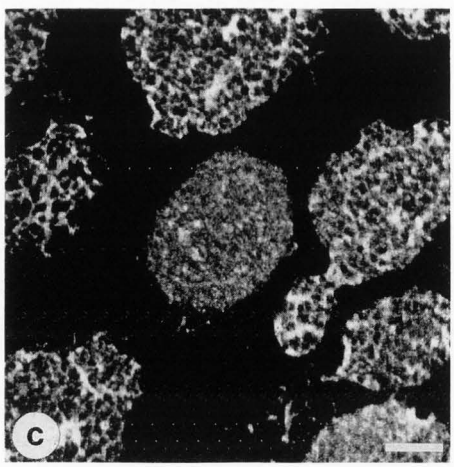

Figure 2. Images from sections of a pellet of murine erythroleukemic cells chemically fixed in the culture medium, centrifuged, frozen, lyophilized and embedded in Spurr resin.
1024 x 1024 pixels, probe current 70pA.
Bar = 2.5 μm.
a: Topography of a 2 μm thick section where the sectioning produced sections of uneven thickness.
b: CN^- distribution map from the same area as (a). The relief visible on (a) generated edge effects on this CN^- image.
$4.44.10^6$ counts collected in 134s.
c: CN^- map of a flat section from the same block as above. No edge effects are visible.
$2.06.10^6$ counts collected in 67s.

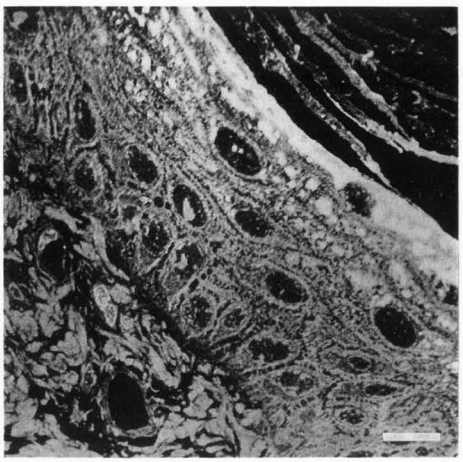

Figure 3. Epon section from a chemically fixed sample of hairless rat skin: histological map (mass 26:CN^-). 512 x 512 pixels, probe current 30 pA. About 35.10^6 counts collected in 525s. Bar = 10 μm. Even at this low magnification it is possible to recognize microstructures in the stratum corneum, the epidermis and dermis.

Imaging the distribution of diffusible elements.

A blood droplet was frozen, lyophilized and embedded in Spurr resin following the protocol described in Materials and Methods; transvers sections were analyzed. Fig.4a is a 20 μm x 20 μm, interlaced acquisition map of K^+ and Na^+ obtained by peak switching (Chabala et al., 1989). Odd numbered lines from 1 to 511 correspond to the Na^+ signal, even lines (2 to 512) correspond to the K^+ signal. This acquisition technique gives after separation two isodepth analytical maps, for K^+ (Fig.4b) and Na^+ (Fig.4c) respectively, acquired under identical instrumental conditions from the same area. Fig 4b shows that K^+ is retained in the erythrocytes, the plasma exhibiting a lower K^+ signal. A network had formed in the plasma due to the growth of ice

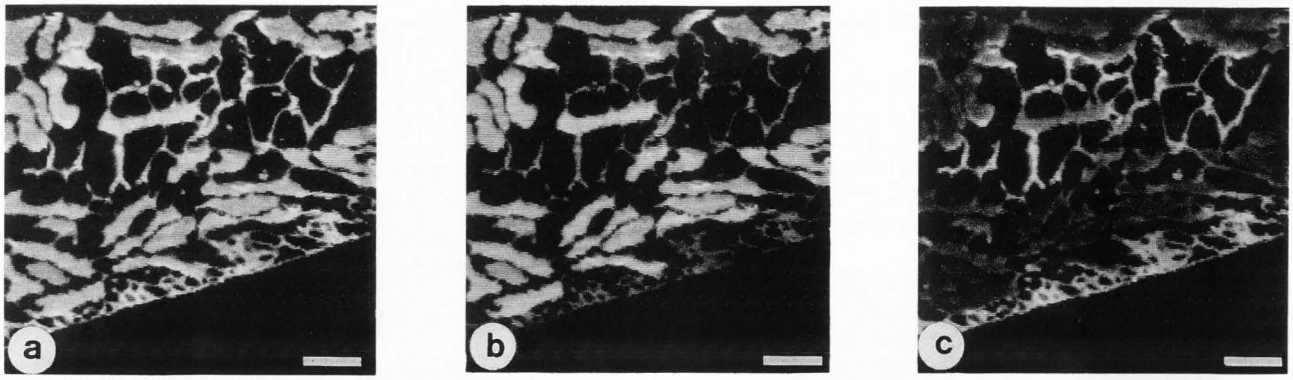

Figure 4. Section of blood sample frozen, lyophilized and embedded in Spurr resin. 512 x 512 pixels, probe current 70 pA. Bar = 3 μm.
a: composite picture where the odd lines 1 to 511 correspond to Na^+ signal and the even lines 2 to 512 to the K^+ signal. For this area, close to the surface contact with the cooling bath, the $K^+$and Na^+ distributions originate from the same depth in the sample. By image processing, the composite picture can be separated into a K^+ map ((b), where odd lines are black) and a Na^+ map ((c), where even lines are black).
b: K^+ map obtained from the composite picture (a). K^+ is mainly emitted from the erythrocytes.
c: Na^+ map obtained from the composite picture (a). Na^+ is mainly emitted from the plasma. Ice crystals are present in the plasma, the size of these crystals increases from the contact area (lower part of the picture) to the interior of the sample .

crystals. These crystals, which displaced ions and proteins along their surface during growth, were larger in the interior of the droplet than at the contact surface with the cooling bath (lower part of the picture). No ice crystals were visible in the erythrocytes. A more intense Na^+ signal was observed to originate from the plasma than from the erythrocytes (Fig.4c), especially near the contact surface. Fig.5 (raw data) represents the variation of the K^+/Na^+ signal ratio for the erythrocytes as a function of depth, from the contact surface with the cooling bath to the interior of the sample. These values were determined by segmentation of the digitally recorded image and classification of the erythrocytes according to their distance from the contact surface. For each erythrocyte the counts per pixel in K^+ and Na^+, and the K^+/Na^+ ratio were computed using the image processing system. The value at 35 μm from the surface is derived from measurements performed on Fig.6a and Fig.6b. These two pictures (40 μm x 40 μm) were acquired using identical instrument settings. At this depth, we observed that ice crystals were now present even in the erythrocytes (Fig.6c, 20 μm x 20 μm). The low K^+/Na^+ ratios at 9 μm and 13 μm depth are due to the presence of some erythrocytes containing high local Na^+ levels (Fig.4c); corrected values, obtained by discarding the erythrocytes with anomalously high Na^+ level, are plotted in Fig.5 (the value at 9 μm depth corresponded to a single erythrocyte isolated in the plasma rich area in the center of the sample).

Another powerful way to get the cellular K^+/Na^+ signal ratio other than from parallel acquisition maps is to take first an histological map of the tissue, to segment the map in order to isolate the erythrocytes, and to scan exclusively the erythrocytes while acquiring a mass spectrum (vector or directed area scan). This mode is especially useful for the acquisition, from the same area, of many isotopic signals (i.e., more than 4 isotopes at the same time,which is the present limitation of our parallel acquisition map system).

We used the latter technique to compute the K^+/Na^+ signal ratio at 55 μm from the contact surface (Fig.5); a portion of the corresponding mass spectrum is shown in

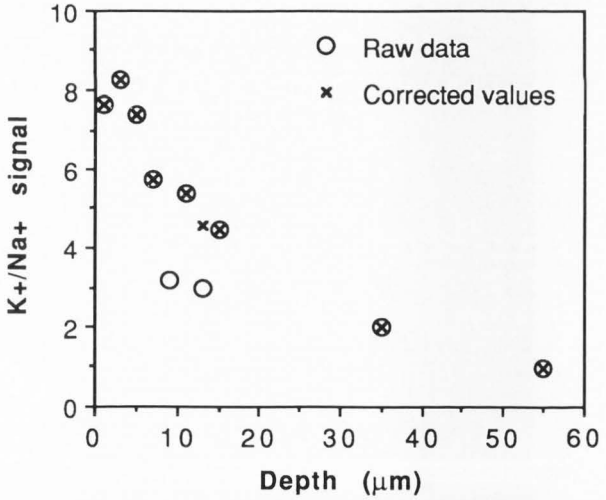

Figure 5. K^+/Na^+ emission ratios from erythrocytes as a function of the distance from the contact surface with the cooling bath.

Fig.7. Fig.8a corresponds to a new area (20 μm x 20 μm) at the contact surface with the cooling bath; here again, K^+ emission was more intense from the red blood cells than from the plasma; in contrast, Na^+ emission was greater from the plasma than from the red blood cells (Fig.8b). The analytical map at mass 56^+ (Fe^+ and CaO^+) (Fig.8c), from the same area as Fig.8a and Fig.8b, shows a signal emitted mainly from the red blood cells. In order to check the contribution of CaO^+ ions to this signal, we acquired a $^{40}Ca^+$ map (Fig.8d) from the same area as Fig.8c. This image reveals an *in vivo*-like distribution of calcium, abundant in the plasma; almost no signal is emitted from the red blood cells. Therefore, Fig.8c

actually shows the Fe^+ distribution in the sample.

Sample embedding medium.

Fig.8e was obtained with the signal at mass 12^+, from the area described above. This signal, presumably due to $^{12}C^+$, was emitted from the organic material as well as from the resin used to embed the sample. Plastic filled up all cavities created by the sublimation of ice crystals. One can also notice that the edges of the structures seen on all the analytical maps previously shown are sharp, even in the case of diffusible elements.

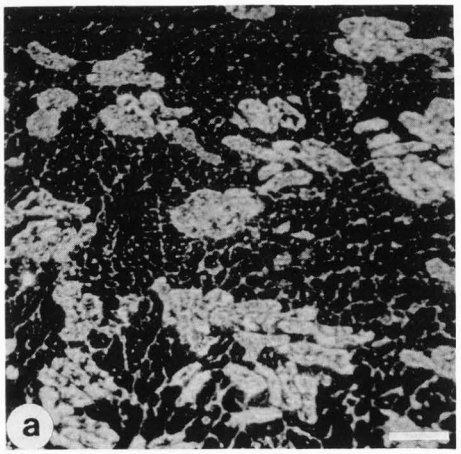

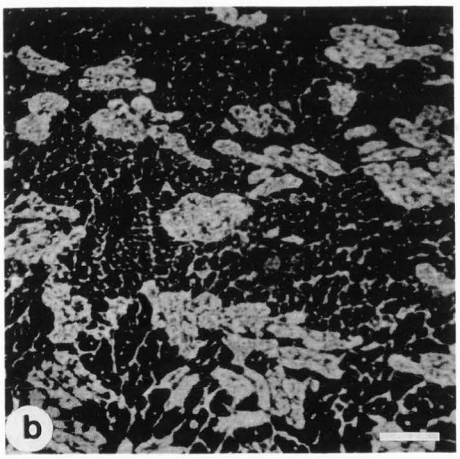

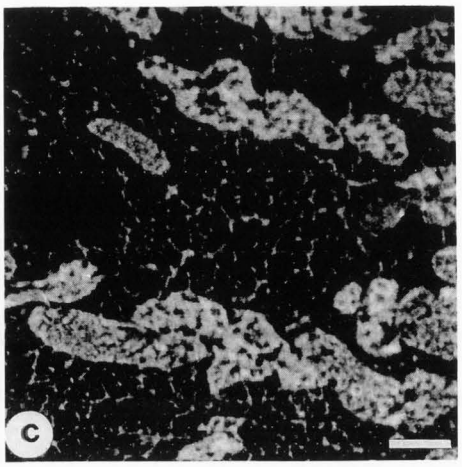

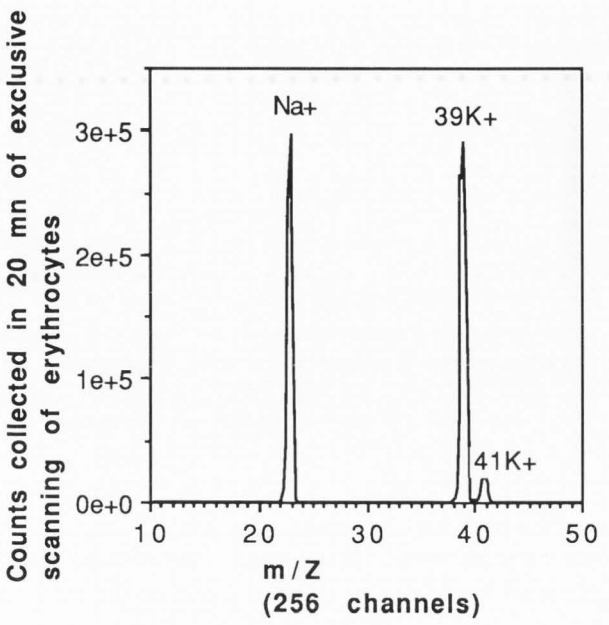

Figure 7. Portion of mass spectrum (from mass 10 to 50) acquired during selected area scans of erythrocytes located at about 55 μm from the contact surface with the cooling bath. The K^+/Na^+ ratio is 0.97.

Discussion

To take full advantage of the high lateral resolution of the analytical maps acquired using the UC-SIM, we need to correlate bioaccumulation of a particular element with the hosting organelles. The analysis of histological maps (CN^-) obtained from chemically fixed samples embedded in plastic (Fig.3) allows us to easily recognize biological structures. As shown in previous studies (Levi-Setti et al., 1988c; Hallégot et al., 1989a), $26CN^-$ maps acquired from lyophylized cryosections exhibit low contrast that precludes a good structure recognition.

Although chemical fixation is well suited when microanalysis is performed to locate an element which is actually a strongly bound constituent of the investigated structure (as is the case for e.g a labelled DNA probe in chromosomes (Hallégot et al., 1989b)), cryofixation is essential for elements that could otherwise be translocated

Figure 6.Sample of blood frozen, lyophilized and embedded in Spurr resin; this area is located at about 35 μm from the contact surface with the cooling bath.
1024 x 1024 pixels, probe current 70 pA. (a) and (b) were acquired using identical instrumental conditions.
a: K^+ image shows similar emission intensity from the erythrocytes and from the plasma.
$3,7.10^6$ counts collected in 34 s. Bar = 5 μm.
b: Sodium picture also shows similar emission intensity from the cells and from the plasma.
$4,33.10^6$ counts collected in 34s. Bar = 5 μm.
c: K^+ image at a higher magnification.Small ice crystals are present in the erythrocytes.
$1,75.10^6$ counts collected in 67 s. Bar = 2.5 μm.

during sample preparation (Morgan et al., 1975; Barnard and Sevéus, 1978; Sevéus, 1978).

Many cryofixation techniques have been developed, the most widely used are jet freezing (Moor et al., 1976; Müller et al., 1980), plunge freezing (Bald,1984; Ryan et al., 1987; Escaig,1982; Elder et al., 1982; Handley et al., 1981), and cold block freezing (Escaig, 1982; Heuser et al., 1979); these techniques have been extensively investigated (for reviews see (Bald, 1985; Costello et al., 1982)). Ideal cryofixation where cell water has been vitrified (Echlin, 1989) minimizes ion

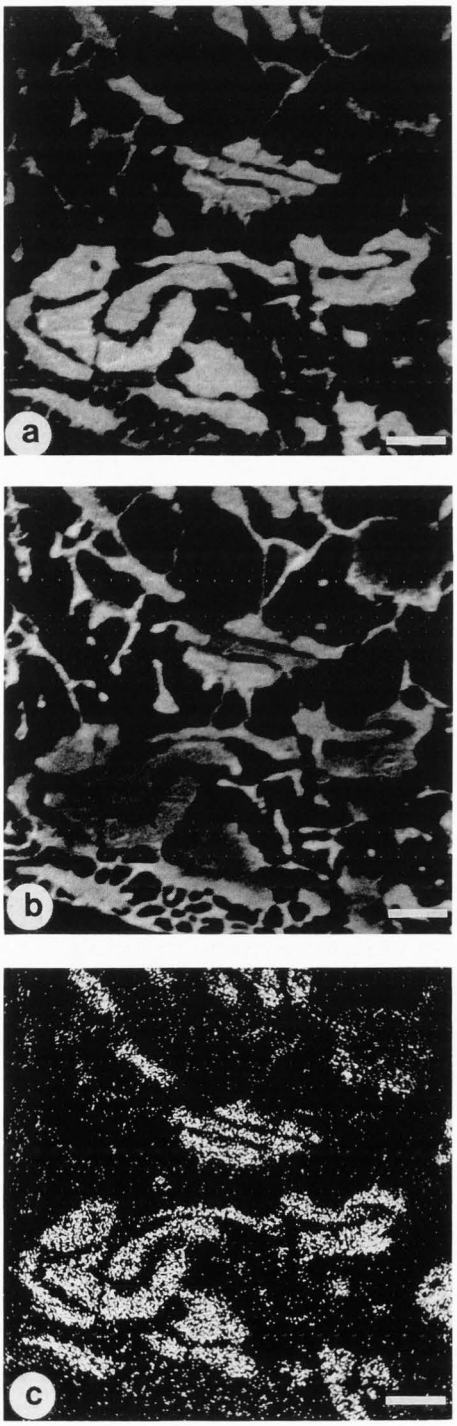

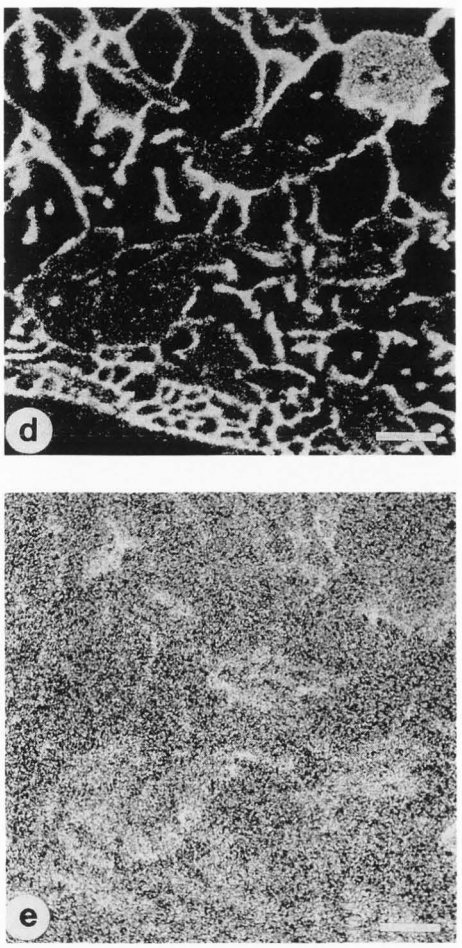

Figure 8. Blood sample frozen, lyophilized and embedded in Spurr resin; study of the contact area with the cooling bath.
Probe current 70 pA. Bar = 2.5 μm.
(a) and (b) were recorded in the same instrumental conditions by peak switching.
a: K^+ image. The potassium signal is more intense from the red blood cells than from the plasma. Ice crystals are present in the plasma.
1024 x 1024 pixels, $3,99.10^6$ counts collected in 67 s.
b: Na+ image. The sodium signal is more intense from the plasma than from the erythrocytes.
1024 x 1024 pixels, $3,76.10^6$ counts collected in 67 s.
c: Fe+ image. Iron in hemoglobin is emitted from the red blood cells.
512 x 512 pixels, 1236 counts collected in 525 s.
d: Ca+ image. The picture shows an in vivo-like distribution of calcium, more abundant in the plasma than in the erythrocytes.
512 x 512 pixels, 165811 counts collected in 525 s.
e: $^{12}C^+$ image. Carbon from tissue and resin is emitted over the entire section, inclusive cavities produced by the lyophilization of ice crystals; this distribution reveals a correct embedding of the sample.
$8,9.10^6$ counts displayed in 525 s.

translocation. However, it is the lateral resolution of the analytical instrument and the physiological process investigated that will determine the best choice for a freezing technique; for example, the mobility of the analyzed element is an important criterion in this choice. In our study, Fe (Fig.8c) and Ca (Fig.8d) present an *in vivo*-like distribution, even in areas where K and Na have not been properly immobilized. There is evidence of ice crystal growth in the highly hydrated plasma, even at the contact surface with the cooling bath where a fine reticulation can be seen. Deeper in the sample, large crystals distorted the shape of the erythrocytes. These ice crystals may have grown during the freezing of the sample, or during its lyophilization at a rather high temperature (-55°C) that allowed ice recristallization. The dramatic regular decrease of the K^+/Na^+ ratio (Fig.5) in erythrocytes as a function of depth from the surface, suggests that ion redistribution took place during the freezing, due to the slowing down of the cooling rate across the sample. The slowing down of the cooling rate with increasing depth is also evident from the presence of small ice crystals in deep erythrocytes (Fig.6). To avoid the problems associated with cryosectioning, cryosubstitution (for a review see Harvey, 1982) is often used to embed biological samples in plastic. Another technique (Burns and File, 1986) consists in freeze drying biological tissue prior to its plastic embedding without using intermediate solvents. In our study, we show that analytical images obtained from samples prepared following the latter embedding technique always present sharp boundaries and that submicromiter cavities due to ice crystal growth in erythrocytes are kept free of Na or K. These observations demonstrate that for our samples, the lateral extent of elemental translocation induced during the embedding technique is comparable or less than the lateral resolution of the UC-SIM and consequently much less than that of a conventional ion microscope. Linner et al. (1986) presented an advanced freeze-drying/embedding apparatus which is commercially available.

Because of its ability to acquire simultaneously high lateral resolution elemental maps, and to quantify secondary ion signals from small selected areas of biological tissue, the UC-SIM offers an original way to evaluate the efficiency of cryofixation methods in regard to the immobilization of diffusible elements.

Acknowledgements

This work was supported by the National Science Foundation under Grant DIR-8610518. We wish to thank Doctor Olivier Hermine from Professor Goldwasser laboratory at the University of Chicago, who provided the murine erythroleukemic cells. L'Oréal research laboratories (Aulnay-Sous-Bois, Paris) provided the skin sample.

References

Bald WB (1984) The relative efficiency of cryogenic fluids used in the rapid quench cooling of biological samples. Journal of Microscopy, 134, 261-170.

Bald WB (1985) The relative merits of various cooling methods. Journal of Microscopy, 140, 17-40.

Barnard T, Sevéus L (1978) Preparation of biological material for X-ray microanalysis of diffusible elements. Journal of Microscopy, 112,, 281-291.

Burns MS (1982) Applications of secondary ion mass spectrometry (SIMS) in biological research: a review. Journal of Microscopy, 127, 237-258.

Burns MS, File DM (1986) Quantitative microlocalization of diffusible ions in normal and galactose cataractous rat lens by secondary ion mass spectrometry. Journal of Microscopy, 144, 157-182.

Burns MS (1988) Biological microanalysis by secondary ion mass spectrometry: status and prospects. Ultramicroscopy, 24, 269-282.

Castaing R, Jouffrey B, Slodzian G (1960) Sur les possibilités d'analyse locale d'un échantillon par utilisation de son émission ionique secondaire (Local analysis from sample secondary ion emission). C. R. Acad. Sciences, 251, 1010-1012.

Castaing R, Slodzian G (1962) Microanalyse par émission ionique secondaire (Microanalysis by secondary ion emission). J. Microscopie, 1, 395-410.

Chabala JM, Levi-Setti R, Wang YL (1988) Practical resolution limits of imaging microanalysis with a scanning ion microprobe. Appl Surf Sci 32, 10-32.

Chabala JM, Levi-Setti R, Wang YL (1989) Advanced imaging and analysis techniques with a scanning ion microprobe. In: Microbeam Analysis-1989, Russell PE (ed.), San-Francisco Press, 586-590.

Chandra S, Morrison GH (1985) Imaging elemental distribution and ion transport in cultured cells with ion microscopy. Science, 228, 1543-1544.

Costello MJ, Fetter R, Höchli M (1982) Simple procedures for evaluating the cryofixation of biological samples. Journal of Microscopy, 125, 125-136.

Echlin P (1989) Cryomicroscopy and analysis: procedures, problems, and prospects. In:Microbeam Analysis-1989, Russel PE (ed.), San-Francisco Press, 79-84.

Elder HY, Gray CC, Jardine AG, Chapman JN, Biddlecombe WH (1982) Optimum conditions for cryoquenching of small tissue blocks in liquid coolants. Journal of Microscopy, 126, 45-61.

Escaig J (1982) New instruments which facilitate rapid freezing at 83K and 6K. Journal of Microscopy, 126, 221-229.

Galle P (1982) Tissue localization of stable and radioactive nuclides by secondary ion microscopy. J. Nucl. Med., 23, 52-57.

Galle P, Berry JP, Escaig F (1983) Secondary ion mass microanalysis: Applications in Biology. Scanning Electron Microsc. 1983; II: 827-839.

Hallégot P, Berry JP, Levi-Setti R, Chabala JM, Galle P (1989a) Metabolism of beryllium: a scanning ion microprobe analysis. Trace Elements in Medicine, 6, 3, 96-103.

Hallégot P, Girod C, Le Beau MM, Levi-Setti R (1989b) High spatial resolution SIMS imaging of labelled human chromosomes. In Secondary Ion Mass Spectrometry, SIMS VII. Benninghoven A, Evans CA, McKeegan KD, Storms HA, Werner HW (eds), John Wiley & Sons, 327-330.

Handley DA, Alexander JT, Chien S (1981) The design and use of a simple device for rapid quench-freezing of biological samples. Journal of Microscopy, 121, 273-282.

Harvey DMR (1982) Freeze-substitution . Journal of Microscopy, 127, 209-221.

Heuser JE, Reese TS, Dennis MJ, Jan Y, Jan L, Evans L (1979) Synaptic vesicle exocytosis captured by quick freezing and correlated with quantal transmitter release. J. Cell Biology, 81, 275-300.

Levi-Setti R, Crow G, Wang YL (1985) Progress in high resolution scanning ion microscopy and secondary ion mass spectrometry imaging microanalysis. Scanning Electron Microsc. 1985; II: 535-551.

Levi-Setti R, Chabala JM, Wang YL (1988a) Aspects of high resolution imaging with a scanning ion microprobe. Ultramicroscopy, 24, 97-114.

Levi-Setti R (1988b) Structural and microanalytical imaging of biological materials by scanning microscopy with heavy-ion probes. Ann. Rev. Biophys. Chem.,17, 325-347.

Levi-Setti R, Berry JP, Chabala JM, Galle P (1988c) Selective intracellular beryllium localization in rat tissue by mass-resolved ion microprobe imaging. Biology of the Cell, 63, 77-82.

Linner JG, Livesey SA, Harrison DS, Steiner AL (1986) A new technique for removal of amorphous phase tissue water without ice crystal damage: a preparative method for ultrastructural analysis and immumoelectron microscopy. J. Histochem.Cytochem., 34, 9, 1123-1135.

Moor H, Kistler J, Müller M (1976) Freezing in a propane jet. (8th Annual Meeting of the Union of Swiss Societies of Experimental Biology, abstract), Experientia, 32, 805.

Morgan A.J, Davies TW, Erasmus DA (1975) Changes in the concentration and distribution of elements during electron microscope preparative procedures. Micron, 6, 11-23.

Müller M, Meister N, Moor H (1980) Freezing in a propane jet and its application in freeze-fracturing. Mikroskopie (Wien), 36, 129-140.

Quettier A, Quintana C (1979) Répartition du carbone organique et inorganique dans les tissus contenant du carbonate de calcium par émission ionique secondaire (Distribution of organic and inorganic carbon in tissue containing calcium carbonate: study by secondary ion emission). C.R. Acad. Sc. Paris, 289, Série D: 433-436.

Ryan KP, Purse DH, Robinson SG, Wood JW (1987) The relative efficiency of cryogens used for plunge-cooling biological specimens. Journal of Microscopy, 145, 89-96.

Sevéus L (1978) Preparation of biological material for X-ray microanalysis of diffusible elements. Journal of Microscopy, 112, 269-279.

Spurr AR (1969) A low-viscosity epoxy resin embedding medium for electron microscopy.Journal of Ultrastructure Research, 26, 31-43.

Discussion with Reviewers

M.S. Burns: How do the authors know, for the cryofixation procedure, that the water was totally removed during the low temperature phase of the drying process and not while the sample was allowed to come to room temperature? If the sample warmed while it was still partially hydrated, the diffusion of electrolytes is possible. This procedure is unlike the one our laboratory has used, in which the sample is maintained at -30°C until after all the water is removed.

G.M. Roomans: Are you certain that the blood samples were completely dry before embedding? Your results indicate that deep in the sample, Na and K must still have been mobile.

Authors: If, despite the high freeze-drying temperature and the small size of the blood droplet (4µl), the samples were not completely dry before warm-up or before embedding, and if the subsequent redistribution of K and Na between plasma and erythrocytes was important enough to cause the observed decrease of the K/Na ratio deep in the sample, an homogenization of the erythrocyte content would have also most likely occur. The fact that submicrometer ion-free areas, corresponding to the growth of small ice crystals in deep erythrocytes (Fig.6), are maintained free of K and Na, strongly suggests that no diffusion occured after the sublimation of the ice crystals.

D.S.Simons: Fig. 6 shows submicrometer lateral localization of Na and K even though K/Na is lower by a factor of 4 compared to the near-surface image. Why isn't the lateral image more diffuse? An implicit conclusion that should be explicitly stated is that good lateral localization in ion maps does not prove that the ions remained stationary during preparation.

Authors: It is true that if the ion diffusion occurs only before the embedding procedure, the ions will, after the removal of water, underline the biological structures of the tissue as it would be the case without diffusion. Therefore, sharp analytical maps do not prove that the ions remained stationary during preparation. However, diffusion during the embedding procedure could generate a concentration gradient along the biological structures, due to the presence of the ions in the plastic matrix that now fills the spaces previously occupied by water.

G.M. Roomans: Have maps based on the signal for phosphorus (phosphate) been tried in order to provide information on morphology?

Authors: Phosphorus maps ($^{79}PO_3^-$) have been used in conventional SIMS, under O_2^+ bombardment, to localize nuclei in embedded tissue sections (Berry et al., 1986). When using the UC-SIM, the phosphate signals (PO^-, PO_2^-, PO_3^-), even acquired from phosphorus rich samples (chromosomes), are typically one to two order of magnitude lower than the CN^- signal. For this reason, and because nuclei and other organelles are already clearly visible in high spatial resolution CN^- images, no attempt has been made to use phosphate signal to get information on morphology.

Additional Reference

Berry JP, Escaig F, Lange F, Galle P. (1986) Ion Microscopy of the thyroid gland: a method for imaging stable and radioactive iodine. Laboratory Investigation, 55, 1, 109-119.